

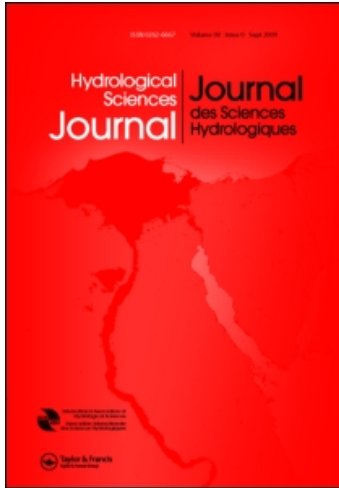
This article was downloaded by:

On: 7 March 2011

Access details: *Access Details: Free Access*

Publisher *Taylor & Francis*

Informa Ltd Registered in England and Wales Registered Number: 1072954 Registered office: Mortimer House, 37-41 Mortimer Street, London W1T 3JH, UK



Hydrological Sciences Journal

Publication details, including instructions for authors and subscription information:

<http://www.informaworld.com/smpp/title~content=t911751996>

The coupled routing and excess storage (CREST) distributed hydrological model

Jiahu Wang^{ab}; Hong Yang^a; Li Li^{ab}; Jonathan J. Gourley^c; Khan Sadiq I.^a; Koray K. Yilmaz^{de}; Robert F. Adler^{de}; Frederick S. Policelli^d; Shahid Habib^d; Daniel Irwn^f; Ashutosh S. Limaye^f; Tesfaye Korme^g; Lawrence Okello^g

^a School of Civil Engineering and Environmental Sciences, University of Oklahoma, Norman, Oklahoma, USA ^b State Key Laboratory of Hydrology - Water Resources and Hydraulic Engineering, Hohai University, Nanjing, China ^c NOAA/National Severe Storm Laboratory, Norman, Oklahoma, USA ^d NASA Goddard Space Flight Center, Greenbelt, Maryland, USA ^e Earth System Science Interdisciplinary Center, University of Maryland, College Park, Maryland, USA ^f NASA Marshall Space Flight Center, Huntsville, Alabama, USA ^g African Regional Centre for Mapping of Resources for Development (RCMRD), Nairobi, Kenya

Online publication date: 13 February 2011

To cite this Article Wang, Jiahu , Yang, Hong , Li, Li , Gourley, Jonathan J. , Sadiq I., Khan , Yilmaz, Koray K. , Adler, Robert F. , Policelli, Frederick S. , Habib, Shahid , Irwn, Daniel , Limaye, Ashutosh S. , Korme, Tesfaye and Okello, Lawrence(2011) 'The coupled routing and excess storage (CREST) distributed hydrological model', *Hydrological Sciences Journal*, 56: 1, 84 – 98

To link to this Article: DOI: 10.1080/02626667.2010.543087

URL: <http://dx.doi.org/10.1080/02626667.2010.543087>

PLEASE SCROLL DOWN FOR ARTICLE

Full terms and conditions of use: <http://www.informaworld.com/terms-and-conditions-of-access.pdf>

This article may be used for research, teaching and private study purposes. Any substantial or systematic reproduction, re-distribution, re-selling, loan or sub-licensing, systematic supply or distribution in any form to anyone is expressly forbidden.

The publisher does not give any warranty express or implied or make any representation that the contents will be complete or accurate or up to date. The accuracy of any instructions, formulae and drug doses should be independently verified with primary sources. The publisher shall not be liable for any loss, actions, claims, proceedings, demand or costs or damages whatsoever or howsoever caused arising directly or indirectly in connection with or arising out of the use of this material.

The coupled routing and excess storage (CREST) distributed hydrological model

Jiahu Wang^{1,2}, Hong Yang¹, Li Li^{1,2}, Jonathan J. Gourley³, Khan Sadiq I.¹, Koray K. Yilmaz^{4,5}, Robert F. Adler^{4,5}, Frederick S. Policelli⁴, Shahid Habib⁴, Daniel Irwn⁶, Ashutosh S. Limaye⁶, Tesfaye Korme⁷ & Lawrence Okello⁷

¹*School of Civil Engineering and Environmental Sciences, University of Oklahoma, Norman, Oklahoma 73019, USA*
yanghong@ou.edu

²*State Key Laboratory of Hydrology – Water Resources and Hydraulic Engineering, Hohai University, Nanjing 210098, China*

³*NOAA/National Severe Storm Laboratory, Norman, Oklahoma 73072, USA*

⁴*NASA Goddard Space Flight Center, Greenbelt, Maryland 20771, USA*

⁵*Earth System Science Interdisciplinary Center, University of Maryland, College Park, Maryland 20740, USA*

⁶*NASA Marshall Space Flight Center, Huntsville, Alabama 35812, USA*

⁷*African Regional Centre for Mapping of Resources for Development (RCMRD), Nairobi, Kenya*

Received 6 April 2010; accepted 5 October 2010; open for discussion until 1 August 2011

Citation Wang, J., Yang, H., Li, L., Gourley, J. J., Sadiq, I. K., Yilmaz, K. K., Adler, R. F., Policelli, F. S., Habib, S., Irwn, D., Limaye, A. S., Korme, T. & Okello, L. (2011) The coupled routing and excess storage (CREST) distributed hydrological model. *Hydrol. Sci. J.* 56(1), 84–98.

Abstract The Coupled Routing and Excess Storage model (CREST, jointly developed by the University of Oklahoma and NASA SERVIR) is a distributed hydrological model developed to simulate the spatial and temporal variation of land surface, and subsurface water fluxes and storages by cell-to-cell simulation. CREST's distinguishing characteristics include: (1) distributed rainfall–runoff generation and cell-to-cell routing; (2) coupled runoff generation and routing via three feedback mechanisms; and (3) representation of sub-grid cell variability of soil moisture storage capacity and sub-grid cell routing (via linear reservoirs). The coupling between the runoff generation and routing mechanisms allows detailed and realistic treatment of hydrological variables such as soil moisture. Furthermore, the representation of soil moisture variability and routing processes at the sub-grid scale enables the CREST model to be readily scalable to multi-scale modelling research. This paper presents the model development and demonstrates its applicability for a case study in the Nzoia basin located in Lake Victoria, Africa.

Key words distributed hydrological model; cell-to-cell routing; excess storage; water balance; CREST; Lake Victoria

Le modèle hydrologique distribué couplé routage et stockage des excédents (CREST)

Résumé Le modèle couplé routage et stockage des excédents (CREST, développé conjointement par l'Université de l'Oklahoma et NASA SERVIR) est un modèle hydrologique distribué développé pour simuler les variations spatiales et temporelles des flux d'eau de surface et souterraine ainsi que les stockages, par simulation de cellule à cellule. Les caractéristiques distinctives de CREST sont les suivantes: (1) production pluie–débit distribuée et routage de cellule à cellule; (2) couplage de la production et du routage du ruissellement via trois mécanismes de rétroaction; et (3) représentation de la variabilité sub-cellulaire de la capacité de stockage en eau du sol et du routage infra-cellulaire (via des réservoirs linéaires). Le couplage entre la genèse du ruissellement et les mécanismes de routage permet un traitement détaillé et réaliste des variables hydrologiques telles que l'humidité du sol. En outre, la représentation de la variabilité de l'humidité du sol et des processus de routage à l'échelle sub-cellulaire permet au modèle CREST d'être facilement étendu à la recherche sur la modélisation multi-échelles. Cet article présente le développement du modèle et démontre son applicabilité pour une étude de cas dans le bassin de la Nzoia, Lac Victoria, Afrique.

Mots clefs modèle hydrologique distribué; routage de cellule à cellule; stockage des excédents; bilan hydrique; CREST; Lac Victoria

1 INTRODUCTION

Knowledge of the spatiotemporal distribution of water over the landscape is of paramount importance for sustainable management of water resources and for mitigating water-related natural hazards such as flooding. Hydrological models serve as important tools for providing critical information in this regard. A variety of hydrological models have been developed in the past (see Singh, 1995, for a comprehensive overview) with various degrees of hydrological processes represented according to the intended application or availability of data. Hydrological models have been classified as conceptual or physically-based (Beck, 1987; Refsgaard, 1996; Yilmaz *et al.*, 2010). Conceptual models represent complex, spatially variable, hydrological processes in a watershed using simple, parsimonious mathematical expressions without explicit treatment of the underlying physics or intra-basin heterogeneity (e.g. Bergström, 1995; Burnash, 1995). Spatially distributed, physically-based hydrological models mathematically represent each of the important components of the hydrological cycle based on their physical governing equations (Woolhiser *et al.*, 1990; Refsgaard & Storm, 1995). The potential strengths of distributed hydrological models are: (a) the ability to account for the intra-basin variability of runoff-producing mechanisms; and (b) the ability to infer model parameter values from geospatial data (e.g. geology, topography, soils, and land cover). A hybrid modelling strategy that maintains a balance between the degree of physical realism and data requirements, so as to provide reliable simulations under a variety of settings, seems to be advantageous.

The Coupled Routing and Excess Storage (CREST) distributed hydrological model represents a hybrid modelling strategy and was recently developed by the University of Oklahoma, USA (<http://hydro.ou.edu>) and NASA SERVIR Project Team (www.servir.net). The CREST model simulates the spatio-temporal variation of water and energy fluxes and storages on a regular grid with the grid cell resolution being user-defined, thereby enabling global- and regional-scale applications. The scalability of CREST simulations is accomplished through sub-grid scale representation of soil moisture storage capacity (using a variable infiltration curve) and runoff generation processes (using linear reservoirs). CREST was initially developed to provide online global flood predictions with relatively coarse resolution, but also applicable at small scales, even for single basins; this paper concentrates and tests the

model at the small scale. It can be driven either by satellite-based precipitation estimates and datasets of potential evapotranspiration, or by raingauge observations, remote sensing platforms such as weather radar, and quantitative precipitation forecasts from numerical weather prediction models. The representation of the primary water fluxes, such as infiltration and routing, are closely related to the spatially-variable landscape characteristics (i.e. vegetation, soil type and topography). The runoff generation component and routing scheme are coupled, thus providing realistic interactions between atmospheric, land surface and subsurface water.

This paper provides a detailed description of each modelling component of the CREST model in Section 2. Section 3 demonstrates a regional application of the model with its very first test basin located in Lake Victoria, Africa. Note that Lake Victoria basin is the focus area of our funded NASA SERVIR-Africa project. Section 4 evaluates the CREST model performance for the presented case study, and a summary and discussion are provided in Section 5.

2 CREST MODEL DESCRIPTION

Similar to many distributed hydrological models, CREST represents a region by dividing it into a number of regular spatial elements (see Fig. 1(c)), which we will refer to hereafter as a “cell”. A flow diagram is given in Fig. 1 that depicts the core of the CREST components: rainfall–runoff generation, evapotranspiration, sub-grid cell routing, downstream routing, and feedbacks between the routing and rainfall–runoff modules. A description and the units of each symbol appearing in the figures and equations of this section are supplied in the Appendix.

The vertical profile of a cell in Fig. 1(a) shows that there are four excess storage reservoirs representing interception by the vegetation canopy and subsurface water storage in the underlying three soil layers. In addition, two linear reservoirs simulate sub-grid cell routing of overland and subsurface runoff separately. In each cell, a variable infiltration curve, originally proposed by Zhao *et al.* (1980), is employed to separate precipitation into runoff and infiltration (see Fig. 1(b)). Figure 1(c) shows a plan view of overland water movement and then channel flow based on flow direction and basin area derived from a digital elevation model (DEM), and Fig. 1(d) shows two cell-to-cell routing modules that move water overland as surface runoff and below ground as subsurface interflow. These modules run in parallel,

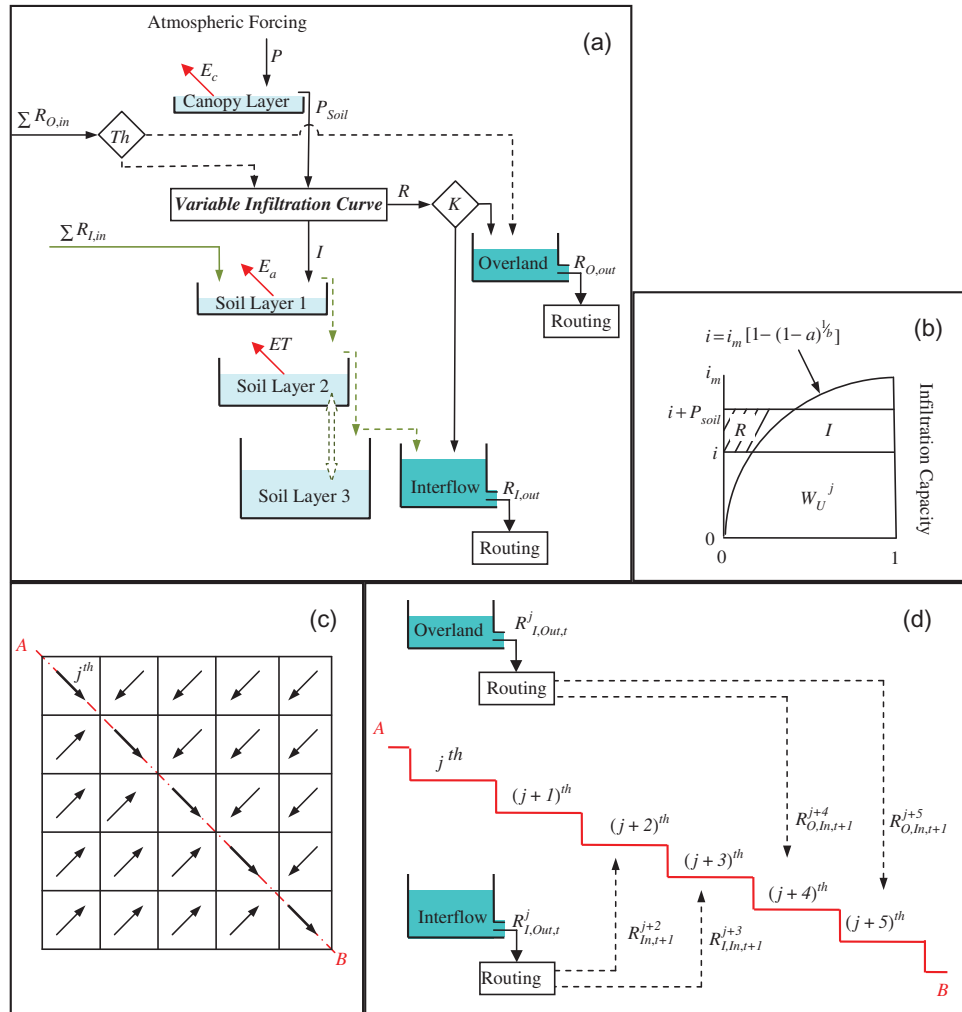


Fig. 1 Core components of CREST: (a) vertical profile of a cell including rainfall–runoff generation, evapotranspiration, sub-grid cell routing and feedbacks from routing; (b) variable infiltration curve of a cell; (c) plan view of cells and flow directions; and (d) vertical profile along several cells including sub-grid cell routing, downstream routing, and subsurface runoff redistribution from a cell to its downstream cells.

which enables a computationally efficient and realistic three-dimensional representation of water flux to downstream cells. The following model description is organized according to the sequential flow of: water entering a cell as rainfall from the atmosphere above; interception by the canopy layer and subsequent redistribution back to the atmosphere via evapotranspiration; division of rainfall reaching the soil surface into infiltration and surface runoff components; sub-grid routing, routing of overland, channel and subsurface components downstream; and, finally, feedbacks between routing and runoff generation components.

2.1 Rainfall–runoff generation

2.1.1 Canopy interception Once there is precipitation (P) input to a cell, the rainfall–runoff

generation process will be activated. First, a portion of the precipitation is intercepted by the vegetation canopy, and an excess storage reservoir is employed here to simulate this process (see Fig. 1(a)). Maximum storage of the reservoir is the canopy interception capacity (CIC): a cell's mean value based on the land cover classification, and modelled based on Dickinson (1989) as follows:

$$CIC = k_c \cdot d \cdot LAI \quad (1)$$

where k_c is the coefficient of the land cover's CIC; d is the vegetation coverage; and LAI is leaf area index. Typically, k_c is set to a value of 1 if the true CIC is accurately estimated from observations or ancillary data; otherwise this coefficient can be calibrated later in rainfall–runoff simulation. When the reservoir

is full, excess precipitation will reach the soil surface:

$$P_{\text{soil}} = P - (\text{CIC} - \text{CI}) \quad (2)$$

where P_{soil} is the precipitation reaching the soil surface and CI is the depth of water intercepted by the vegetation canopy.

2.1.2 Variable infiltration curve Next, P_{soil} is separated into two parts: excess rain (R) and infiltration water (I), according to the variable infiltration curve (VIC; also called tension water capacity curve), founded in the Xinanjiang model (Zhao *et al.*, 1980; Zhao, 1992), and later employed in the University of Washington VIC model (Liang *et al.*, 1996) (see Fig. 1(b)). The curve is:

$$i = i_m \left[1 - (1 - A)^{1/b_i} \right] \quad (3)$$

where i is the point infiltration capacity; i_m is the maximum infiltration capacity of a cell; A is the fractional area of the cell corresponding to i ; and b_i is the exponent of the curve. In equation (3), i_m is a function of the cell's maximum water capacity (W_m) of the three soil layers, as:

$$i_m = W_m (1 + b_i) \quad (4)$$

$$W_m = W_{m1} + W_{m2} + W_{m3} \quad (5)$$

where W_{m1} , W_{m2} and W_{m3} correspond to the three soil layers and are related to soil porosity. Equation (3) can be rewritten as a function of the cell's total mean water of the three soil layers (W), as follows:

$$i = i_m \left[1 - \left(1 - \frac{W}{W_m} \right)^{\frac{1}{1+b_i}} \right] \quad (6)$$

$$W = W_1 + W_2 + W_3 \quad (7)$$

where W_1 , W_2 and W_3 are the mean soil water depth of each layer in the cell. The amount of water available for infiltration (I) is then computed as follows:

$$\text{for } i + P_{\text{soil}} \geq i_m \quad I = (W_m - W)$$

$$\text{for } i + P_{\text{soil}} < i_m$$

$$I = (W_m - W) + W_m \left[1 - \frac{i + P_{\text{soil}}}{i_m} \right]^{1+b_i} \quad (8)$$

There are three storage reservoirs in this model representing three different soil layers. Infiltration water (I) enters the upper soil layer until it is full. The middle and lower soil layers are filled in sequence.

2.1.3 Runoff generation Given the partitioning of P_{soil} into I using equations (3)–(8), the excess rain (R) is computed as:

$$R = P_{\text{soil}} - I \quad (9)$$

A further partitioning of R into overland excess rain (R_O) and interflow excess rain (R_I) ensues by comparing P_{soil} to the infiltration rate of the first layer (K):

$$\text{for } P_{\text{soil}} > K \quad R_I = K \frac{R}{P_{\text{soil}}} \quad R_O = R - R_I \quad (10)$$

$$\text{for } P_{\text{soil}} \leq K \quad R_I = R \quad R_O = 0$$

where K is closely related to the soil saturated hydraulic conductivity. The partition of overland and interflow excess rain provides quick and slow hydrograph responses to precipitation. The terms R_O and R_I are handled separately in the routing component described in Section 2.2.

2.1.4 Evapotranspiration The process of water flux from the land surface soils, vegetation, or directly from overland water to the atmosphere is referred to as evapotranspiration. Potential evapotranspiration (E_p) is the amount of evapotranspiration that would occur if there were an unlimited supply of land surface water, and is often estimated from atmospheric thermodynamics, wind and radiation conditions. The method for estimating E_p in the CREST model depends on the availability of data in the study basin. When radiation data are available, the Priestley-Taylor equation (Priestley & Taylor, 1972) is recommended. If only temperature data are available, the Hargreaves equation (Hargreaves & Samani, 1982) can be used to estimate E_p . In situations where no meteorological data (except rainfall) are available, users can defer to the 0.25-degree monthly mean E_p data available from the Famine Early Warning Systems Network (FEWS NET; <http://igskmncnwb015.cr.usgs.gov/Global/>), which is provided with the CREST software package.

Actual evapotranspiration (E_a) is determined by both E_p and the vertically-integrated water contents of the cell. The process of evapotranspiration begins to remove water from the uppermost canopy reservoir and continues until this storage tank is completely

depleted (i.e. CI from equation (2) goes to 0), with successive drying of Layer 1, and so on:

$$\begin{aligned} \text{for } CI > E_p \quad E_c &= E_p \\ \text{for } CI \leq E_p \quad E_c &= CI \end{aligned} \quad (11)$$

where E_c is the water lost from the canopy layer via evapotranspiration. Next, we define the potential evaporation that applies to the uppermost soil layer (E_{p1}) as follows:

$$E_{p1} = E_p - E_c \quad (12)$$

In the process of the canopy reservoir being depleted, we see that E_{p1} is initially 0, and eventually approaches E_p when the canopy layer is completely devoid of water. In other words, this term activates as the storage tank empties from above. Analogous to the treatment of the depletion of water in the canopy layer in equation (9), the rate of water evaporated from soil layer 1 (E_{s1}) is defined as:

$$\begin{aligned} \text{for } W_1 > E_{p1} \quad E_{s1} &= E_{p1} \\ \text{for } W_1 \leq E_{p1} \quad E_{s1} &= W_1 \end{aligned} \quad (13)$$

where W_1 is the depth of water in the upper soil layer reservoir (refer to equation (7)). The potential evaporation that applies to the second soil layer (E_{p2}) is defined as:

$$E_{p2} = (E_{p1} - E_{s1}) \sqrt{\frac{W_2}{W_{m2}}} \quad (14)$$

From equations (13)–(14), we see that E_{p2} activates in response to a depletion of water in the uppermost soil layer (W_1); the process of drying out the soil column begins from the top and proceeds downward. A reduction term has been included on the right hand side of equation (14) in the calculation of E_{p2} so that it will be less than or equal to E_{p1} (and E_p). Physically, this term represents the increasing difficulty to evaporate water from greater depths in the soils. The rate of actual water evaporated from layer 2 (E_{s2}) in CREST is calculated as:

$$\begin{aligned} \text{for } W_2 > E_{p2} \quad E_{s2} &= E_{p2} \\ \text{for } W_2 \leq E_{p2} \quad E_{s2} &= W_2 \end{aligned} \quad (15)$$

Recall that W_2 is the depth of water in the second soil layer reservoir (see equation (7)). Finally, as the water contents in the second layer are depleted, the

potential evaporation for the third soil layer (E_{p3}) is computed as:

$$E_{p3} = (E_{p2} - E_{s2}) \frac{W_3}{W_{m3}} \quad (16)$$

In this case, the reduction term is larger on the right-hand side than in equation (14) so that E_{p3} will fall below E_{p2} at a higher rate than occurs in the second soil layer. Again, physically, this term represents the additional difficulty encountered in evaporating water with increasing depth. The depletion of water from soil Layer 3 occurs at the following rates:

$$\begin{aligned} \text{for } W_3 > E_{p3} \quad E_{s3} &= E_{p3} \\ \text{for } W_3 \leq E_{p3} \quad E_{s3} &= W_3 \end{aligned} \quad (17)$$

where E_{s3} is the rate of evaporation from soil Layer 3. The vertically-integrated, actual rate of evapotranspiration of a cell is computed as:

$$E_a = E_c + E_{s1} + E_{s2} + E_{s3} \quad (18)$$

The terms in equation (18) are coordinated so that drying and wetting begin from the canopy layer and proceed downward (see Fig. 1(a)). Evapotranspired water is lost to the atmosphere and is no longer considered in the water budget. Deep-layer transpiration by root uptake is not considered in CREST, which currently has a model structure designed for warm season flood simulation.

2.2 Runoff routing

2.2.1 Sub-grid-scale routing

Disadvantages of cell-to-cell routing schemes have been reported and have, in part, motivated the present research. First, most cell-to-cell routing methods do not explicitly account for routing of runoff within a cell, which we refer to herein as sub-grid-scale routing. An example is the modelling of braided streams which meander at scales not easily resolved with commonly available DEMs and must be parameterized. The representation of runoff routing at the sub-grid scale becomes much more problematic with coarser grid scales encompassing global-scale applications (Naden, 1993). In CREST, we employ two linear reservoirs to simulate sub-grid cell routing.

Virtual reservoirs have been incorporated in hydrological modelling studies to account for floodplain storage, groundwater flow, storage by lakes and wetlands, and simulation of operations of real reservoirs (Vörösmarty *et al.*, 1989; Liston *et al.*, 1994;

Coe, 1997; Hagemann & Dümenil, 1997). Interflow and overland excess rain (R_I and R_O ; refer to Section 2.1.3) enter the two linear reservoirs separately as shown in Fig. 1(a), and the reservoir depths are computed as follows:

$$S_{O,t+1} = S_{O,t} + R_{O,t} \quad (19)$$

$$S_{I,t+1} = S_{I,t} + R_{I,t} \quad (20)$$

where the subscript t indicates the time step; S_O is the overland reservoir depth; and S_I is the interflow reservoir depth. Discharge from the overland and subsurface reservoirs, referred to hereafter as overland runoff ($R_{O,out}$) and interflow runoff ($R_{I,out}$), are calculated separately based on a linear model as follows:

$$R_{O,out} = k_O \cdot S_O \quad (21)$$

$$R_{I,out} = k_I \cdot S_I \quad (22)$$

where k_O and k_I are the overland and interflow reservoir discharge parameters, which are a function of the watershed characteristics (such as basin area and slope) and modelling cell size. However, these parameters are often determined through parameter calibration. The outputs from the reservoirs, $R_{O,out}$ and $R_{I,out}$ are passed into the downstream routing module.

2.2.2 Downstream routing The typical approach to routing involves determining the depth and momentum of overland water that flows from each cell to a neighbouring cell downstream and continuing this process down to the river network where it is considered open channel flow (Vörösmarty *et al.*, 1989; Liston *et al.*, 1994; Miller *et al.*, 1994; Sausen *et al.*, 1994; Coe 1997; Hagemann & Dümenil 1997; Branstetter & Famiglietti 1999). The routing component in CREST is based on a two-layer scheme describing overland runoff and interflow from one cell to the next one downstream, with consideration of open channel flow. Advantages of cell-to-cell routing schemes include the ease with which they can be implemented globally (e.g. Miller *et al.*, 1994; Sausen *et al.*, 1994; Coe 1997; Hagemann & Dümenil 1997; Branstetter & Famiglietti 1999); and the explicit accounting of the volume of river water in each cell. This second advantage enables hydrograph computation at any interior cell. Furthermore, when the volume of river water stored in a cell is transformed into a fraction of land area covered by

the surface water (i.e. wetlands, floodplain storage, rivers, lakes, or reservoirs as in Coe, 1997), then the effect of that surface water on land–atmosphere interaction can have feedbacks to climate simulations (Bates *et al.*, 1993; Hostetler *et al.*, 1993; Bonan, 1995; Kundzewicz and Stakhiv, 2010).

The concentration time (T) for $R_{I,out}$ and $R_{O,out}$ is calculated as follows:

$$T^j = \frac{\bar{l}^j}{K_X \sqrt{S^j}} \quad (23)$$

where the superscript j refers to the spatial index of a cell, as illustrated in Fig. 1(c) and (d); T^j is the concentration time from the j th cell to its downstream ($j + 1$)th cell; \bar{l}^j is the distance between the centres of the j th and ($j + 1$)th cells; S^j is the slope from the j th to the ($j + 1$)th cell; and K_X is defined as the runoff velocity coefficient. The value of K_X varies from cell to cell and within cells depending on the following three processes that it represents: for interflow runoff ($R_{I,out}$), K_X is set to a value representative of the soil saturated hydraulic conductivity; for overland runoff ($R_{O,out}$), K_X corresponds to the land surface roughness; and for overland runoff ($R_{O,out}$) where the drainage area of the j th cell exceeds an experimentally-found threshold (Th) (i.e. channel flow), K_X is a channel velocity coefficient determined by the channel roughness and hydraulic radius.

Figure 1(d) illustrates how runoff from interflow, overland flow and channel flow contribute to cells downstream from the j th cell after a time step dT . The $R_{I,out}$ moves more slowly in response to a relatively small value of K_X , corresponding to soil saturated hydraulic conductivity, and provides runoff to the nearby ($j + 2$)th and ($j + 3$)th cells. In contrast, $R_{O,out}$ contributes runoff to the ($j + 4$)th and ($j + 5$)th cells further downstream due to a larger value of K_X . All values for K_X , which control the timing of peak flow, can be provided *a priori* using land cover maps, soil surveys and channel cross-sections, but typically must be optimized through calibration.

2.3 Coupling rainfall–runoff generation and routing

For each cell, the water balance is computed as follows:

$$\begin{aligned} \frac{dSto}{dt} = & P - E_a + \sum R_{O,in} - R_{O,out} \\ & + \sum R_{I,in} - R_{I,out} \end{aligned} \quad (24)$$

where Sto is the total cell water storage, which includes all water stored in the overlying vegetation canopy, the three soil layers, and in the two linear reservoirs (see Fig. 1(a)). The summations for interflow and overland flow in equation (24) correspond to contributing runoff of multiple upstream cells (as determined from values of K_X ; see Fig. 1(d)) and from eight possible flow directions (as determined from a DEM-derived flow direction map; see Fig. 1(c)).

In CREST, routed water from a cell impacts the rainfall–runoff generation as well as routing components of downstream cells, thus coupling these processes in the following three ways. First, overland runoff coming from upstream cells is treated the same as adding precipitation directly on the uppermost soil layer, so that P_{soil} calculated from equation (2) is adjusted as follows:

$$\hat{P}_{soil} = P_{soil} + \sum R_{O,in} \quad (25)$$

where \hat{P}_{soil} is the adjusted P_{soil} as dictated by the total amount of overland flow from upstream cells. This additional water is available to enter the soil layers from above, as described in Section 2.1.2. Secondly, soil moisture is increased by lateral interflow coming from upstream cells, so the amount of water available for infiltration in equation (8) is adjusted as:

$$\hat{I} = I + \sum R_{I,in} \quad (26)$$

where \hat{I} is the adjusted I determined by the sum of interflow from upstream cells. Finally, channel runoff coming from upstream cells contributes to the cell's overland reservoir depth, so that S_O in (19) is modified as follows:

$$\hat{S}_O^{t+1} = S_O^t + R_O^t + \sum R_{O,in} \quad (27)$$

where \hat{S}_O^{t+1} is the adjusted S_O^{t+1} , increased by contributing channel runoff.

These runoff routing-generation feedback mechanisms (i.e. water routed from upper grids could potentially increase runoff generation of the lower grids), via linking the runoff generation and routing modules in CREST, mark it as a distinguishing characteristic from other hydrological models. Because a cell is pre-determined as being a channel cell based on its basin area, only one of the overland runoff processes can occur (i.e. the process in (25) cannot occur simultaneously with that in (27), but either can occur along with (26)). These feedbacks

cause downstream cells to become more readily saturated than upstream cells; a desirable characteristic in excess storage theory is the expansion of the soil saturation area beginning downstream and working its way up (Zhao, 1992). The CREST approach of module coupling enables realistic fluxes of water both horizontally and vertically through the soil structure and laterally overland. Nevertheless, the actual modelling performance also depends upon the accurate quality of soil information such as depth and types.

2.4 Parameter estimation

Many of the parameters in the CREST model can be estimated based on the availability of field survey data, such as soil surveys, land cover maps and vegetation coverage. Other parameters, such as flow direction, slope and drainage area, are derived directly from a DEM. These physically-based parameters are listed in the Appendix (Table A1), along with a suggested source of data to estimate them. There are approximately ten parameters that are much more difficult to estimate from ancillary data and need to be calibrated either manually, automatically, or using combined approaches given observations of rainfall and streamflow. Table A2 in the Appendix lists these parameters, their units and default values.

Conceptual hydrological models are tailored to a specific application through a process of calibration (e.g. Linsley *et al.*, 1986; Beven & Binley, 1992; Gupta *et al.*, 1998; Vrugt *et al.*, 2005). In this process, model parameters are adjusted in successive model simulations until the model output matches the observations to within a previously determined error criterion or multiple criteria. While initial parameter estimates are supplied with the model, we recommend further optimization using either manual calibration or an automatic calibration routine (such as in Reichold, *et al.*, 2010), the latter being supplied with the model. The auto-calibration routine embedded in CREST performs global optimization of the parameter values based on an Adaptive Random Search method (ARS) (Brooks, 1958).

2.5 Inputs and outputs

The two input data sources required to run CREST are: rainfall data and potential evapotranspiration (E_p). The CREST software package comes with a global, climatologically-averaged E_p data set (i.e. FEWS NET). As discussed in Section 2.1.4, better accuracy in estimating E_p can be accomplished with

the availability of atmospheric observations such as temperature, humidity, wind speed, and radiation.

The CREST outputs consist of several variables, all of which are listed in the Appendix (Table A3), including storage depths of the vegetation canopy, the three soil layers, and two linear reservoirs, relative change of the six reservoir levels representing actual evapotranspiration from the canopy and soil layers, overland and interflow excess rain, and overland and interflow runoff. Each variable to be output is selected in a control file and is subsequently written to a 2-D file at a designated frequency. In addition, other variables that are not listed in Table A3 (e.g. re-distribution coefficient) can also be output with a simple modification to the CREST source code, which is provided with the software package written in Fortran 95 and C. The output variables listed in Table A3 can support hydrological research as envisaged by the authors.

3 CREST MODEL IMPLEMENTATION

The CREST model was designed to enable multi-scale hydrological modelling and hence is suited for simulations ranging from coarse scale (grid size of tens of kilometres) to relatively fine resolution (grid

size of 1 km to a few kilometres). In this section we demonstrate the utility of CREST for a regional 1-km fine scale application focusing on the Nzoia Basin in East Africa, which is the first test basin of the CREST model.

3.1 Nzoia River basin

Frequent flooding is a serious problem in East Africa, particularly in the Lake Victoria basin, which affects the lives of 30 million people (Osano *et al.*, 2003). The region around Lake Victoria is prone to high societal impacts from flooding because of the concurrence of extreme rainfall, overflowing tributary rivers and streams, and a high population density. People in the heavily populated regions of Kenya, Uganda and Tanzania live under a threat of flooding almost every year. In late May of 2002 alone, widespread flooding throughout Kenya displaced up to 60 000 people.

The Nzoia River basin, a sub-basin of the Lake Victoria basin, was chosen as the study area because of its territorial, geographic and epidemiological importance for the region (Li *et al.*, 2009). The Nzoia River basin, situated in East Africa, covers approximately 12 696 km², and drains into Lake Victoria (Fig. 2). It is bounded by the latitudes 34°–36°E

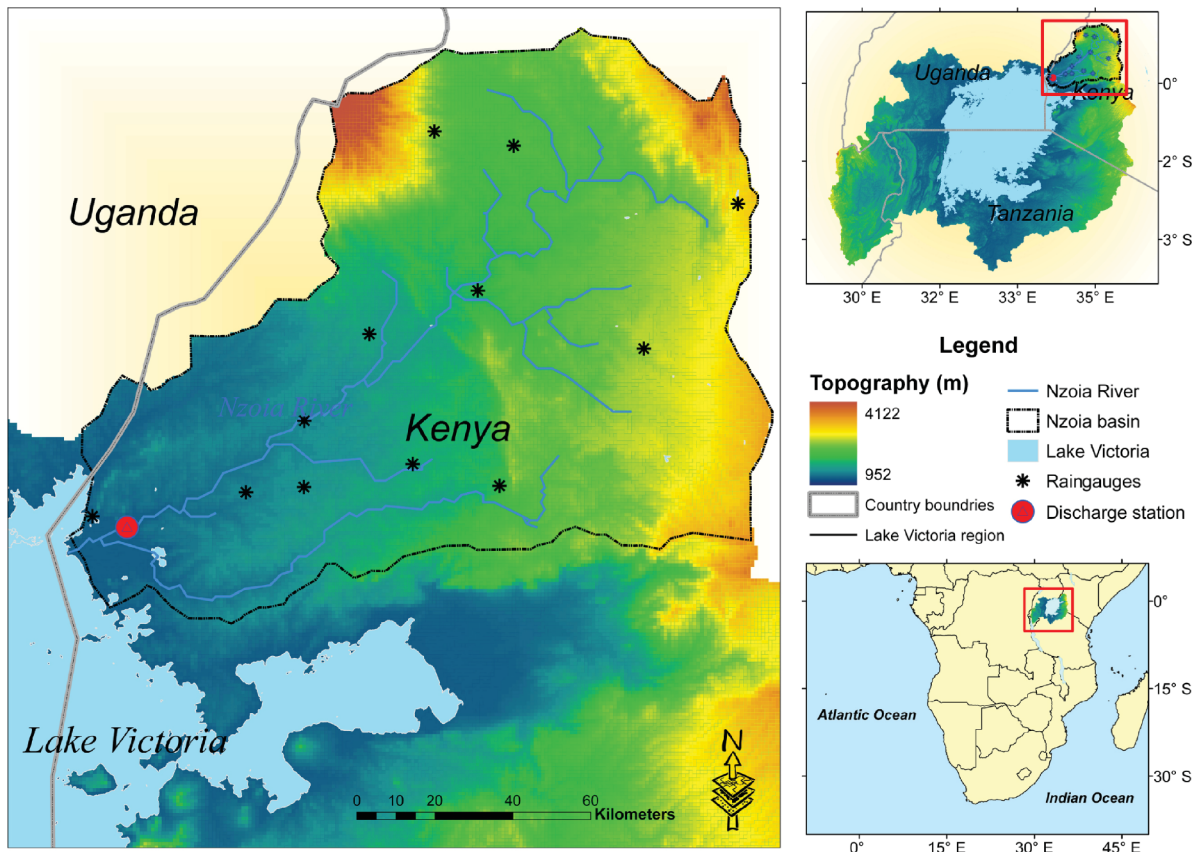


Fig. 2 Study area and rain gauge stations.

and longitudes 0°03'–1°15'N, and the basin elevation ranges from 1134 to 2700 m. It encompasses three geographical regions: the highlands around Mount Elgon and the Cherangany Hills, the upper plateau, which includes Eldoret, and the lowlands. The lowlands are characterized by clayey soils, typical of the greater area, while the highland and upper plateau soils are deeper and well-drained. The predominant soil texture on the basin is clay soils at 77% followed by sandy soils at 14%. The region as a whole receives an average of 1350 mm of rain annually. Annual rainfall in the lowlands is smaller with average amounts of 1076 mm, which increases with elevation reaching 2235 mm in the highlands. The seasonality of the rainfall is predominantly controlled by the movement of the inter-tropical convergence zone (ITCZ). March to May are the primary rainy months while there is a secondary rainy season from October to December. Crop production in the Nzoia basin is important for its cereal and sugar cane yield, producing at least 30% of the national output of both maize and sugar. The total length of the river is 252 km with an average gradient of 4 m km⁻¹.

3.2 Data and model implementation

The key data sets enabling the implementation of the CREST distributed hydrological model in the Nzoia basin in 30 arc-second-resolution, DEM from the Shuttle Radar Topography Mission (SRTM; Rabus *et al.*, 2003; <http://www2.jpl.nasa.gov/srtm/>), SRTM-derived hydrological parameter files of HydroSHEDS (Lehner *et al.*, 2008), soil parameters provided by the Food and Agriculture Organization of the United Nations (FAO; <http://www.fao.org/AG/agl/agll/dsmw.htm>) and the Moderate Resolution Imaging Spectroradiometer (MODIS) land classification map. The latter is used as a surrogate for land use/cover, with 17 classes of land cover according to the International Geosphere–Biosphere Programme classification (Friedl *et al.*, 2002).

The CREST model was implemented at 1-km grid cell resolution for the Nzoia basin and driven by daily precipitation from 12 stations in the basin (see Fig. 2). Observed discharge data from one downstream station (Fig. 2) was employed as a benchmark. Station-based precipitation data were interpolated to the model grid cells based on the Thiessen polygon method. The observed discharge data is available for the period of 1985–2004 at a daily time step.

4 CREST MODEL EVALUATION AND DEMONSTRATION

4.1 Performance in discharge simulation

4.1.1 Evaluation indices CREST simulation performance was assessed using three commonly-used statistical indices. First, for statistical goodness of fit of simulated flows, we utilized the Nash-Sutcliffe coefficient of efficiency (NSCE; Nash & Sutcliffe, 1970):

$$\text{NSCE} = 1 - \frac{\sum (Q_{i,o} - Q_{i,c})^2}{\sum (Q_{i,o} - \bar{Q}_o)^2} \quad (28)$$

where $Q_{i,o}$ is the observed discharge of the i th day; $Q_{i,c}$ is the simulated discharge of i th day; and \bar{Q}_o is the average of all the daily observed discharge values. If $\text{NSCE} \leq 0$, then the model provides no skill in relation to using the observed mean as a predictor. Second, the Pearson Correlation Coefficient (CC) is used to assess the agreement between simulated and observed discharge as follows:

$$\text{CC} = \frac{\sum (Q_{i,o} - \bar{Q}_o)(Q_{i,c} - \bar{Q}_c)}{\sqrt{\sum (Q_{i,o} - \bar{Q}_o)^2 \sum (Q_{i,c} - \bar{Q}_c)^2}} \quad (29)$$

where \bar{Q}_c is the average of all daily simulated discharge values. Third, relative bias ratio assesses the systematic bias of the simulated discharge:

$$\text{Bias} = \frac{\sum Q_{i,c} - \sum Q_{i,o}}{\sum Q_{i,o}} \times 100\% \quad (30)$$

The best skill occurs with $\text{NSCE} = 1$, $\text{CC} = 1$, and $\text{Bias} = 0\%$.

4.1.2 Model calibration and validation

CREST was calibrated using daily observed discharge data for the period between 1985 and 1999. A one-year period (1984) was used for warming up the model states. CREST calibration, performed using the ARS method described in Sec. 2.4, resulted in good performance with $\text{NSCE} = 0.72$, $\text{CC} = 0.89$ and $\text{Bias} = -0.07\%$. Figure 3(a) shows the precipitation and streamflow time series during the calibration and validation time periods, and Fig. 3(b) shows accumulated discharge of observation and simulation. After CREST parameters were calibrated and then fixed, simulations during the validation period from 2000–2004 were excellent as compared to observations with only minor reductions in the NSCE, CC and Bias

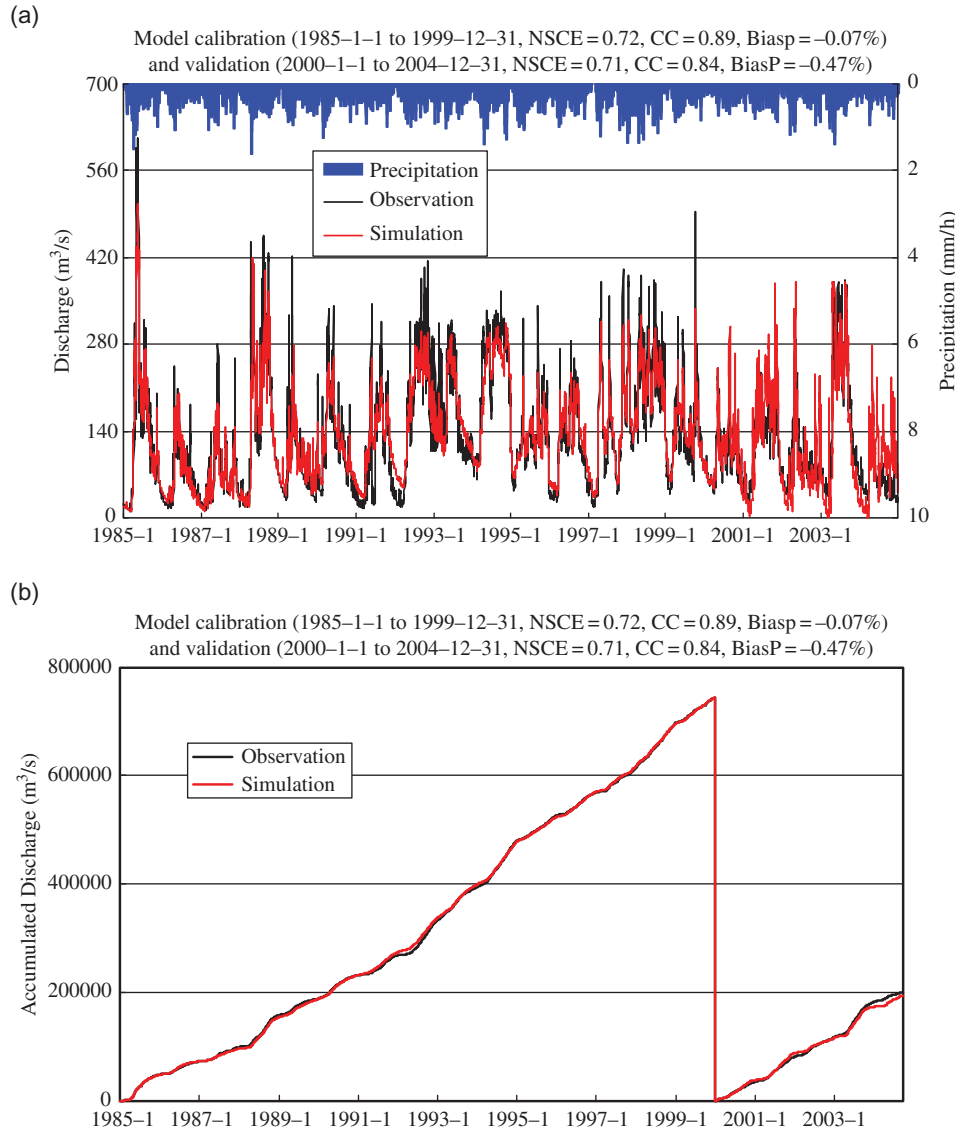


Fig. 3 Comparison of simulated and observed discharge during the calibration and validation periods: (a) discharge time series, and (b) accumulated discharge time series.

error statistics from the values obtained during the calibration period. The error metrics (NSCE = 0.71, CC = 0.84 and Bias = -0.47%) indicate that the CREST model can effectively and robustly reproduce observed discharge in the Nzoia basin.

4.2 Spatially distributed discharge simulation

An important advantage of spatially distributed hydrological models, such as CREST, is that they not only provide estimates of hydrological variables at the basin outlet, but also at any location (represented by a cell) within the basin. As described in Section 2.5, CREST can output any of the variables listed in the Appendix (Table A3) as a raster grid for any time period. As an example, we show in Fig. 4(a) how daily rainfall of the order of 80 mm impacted the upper part

of the Nzoia basin on 22 April 2003. This display of the model inputs also shows the unnatural rainfall patterns that can result from the Thiessen polygon interpolation method. Figure 4(b) shows the cell-by-cell discharge response throughout the basin. We can see how relatively high flows were being experienced near the basin outlet from previous rainfall, with a new flood peak responding to the recent rainfall in the upper part of the basin. If observations are available within the basin, such as soil moisture, then different components of the CREST model can be evaluated.

4.3 Impacts of coupling rainfall-runoff generation and routing components

Most distributed hydrological models consider routing as a separate process following the rainfall-runoff

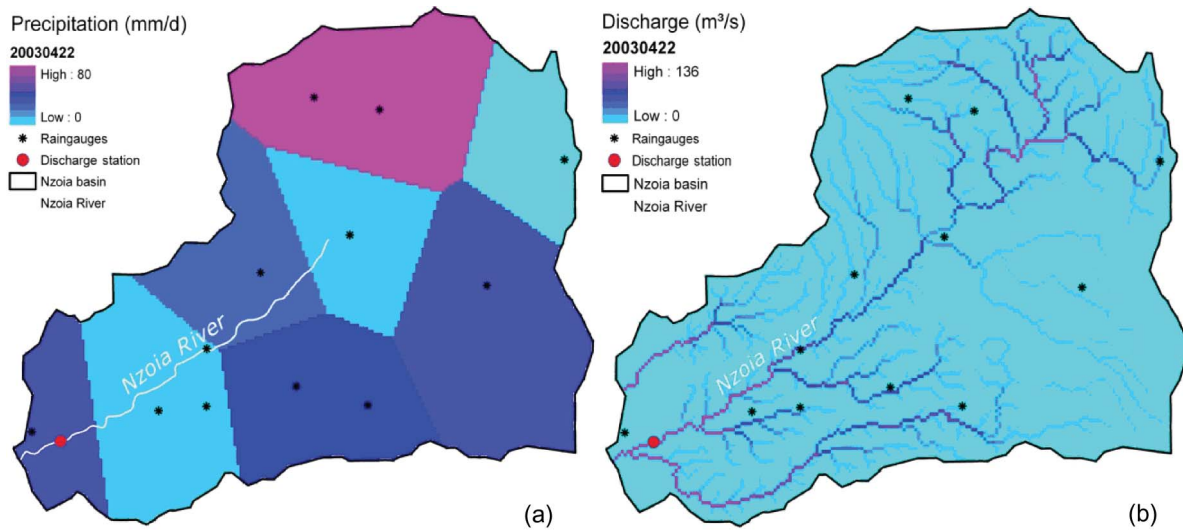


Fig. 4 Example of CREST's display of input data and simulation results in raster format: (a) precipitation on 22 April 2003 (interpolated by Thiessen polygon method), and (b) simulated discharge on every 1-km cell.

generation component. In a synthetic setting in which rain falls uniformly over cells with the same initial soil moisture contents and potential evapotranspiration rates, the excess rain simulated across the basin will be homogenous. This overland and subsurface runoff will be transferred to the routing component which will then move the water overland and in channels until it leaves the basin. In most hydrological models, once surface runoff enters the routing component it no longer is capable of contributing to the soil moisture contents of downstream cells. CREST couples these components so that overland runoff from upstream cells enter the soil moisture reservoirs of downstream cells, and have the effect of saturating cells in low-lying areas (e.g. valleys) first and then propagating upstream.

A synthetic experiment was designed in CREST in order to demonstrate the impacts of coupling the rainfall–runoff generation and routing modules. The spatial distribution of the model parameters and subsequent analysis of raster-based outputs will have variability that results from spatially distributed soil types, land cover, etc.; i.e. variability that is not due to process coupling. In order to highlight impacts due to coupling alone, we designed the experiment under the condition of spatially uniform parameter values, with the exception of the DEM-derived parameters (refer to Appendix, Table A1). The experiment was performed with initial soil moisture contents at zero for all grid cells, spatially homogenous soil types and land cover, and E_p of 5 mm/d. Forcing was from uniform rainfall at a rate of 10 mm/d for 200 consecutive hours, and then turned off. Spatially uniform values

of the parameters in the Appendix (Table A2) were determined from the automatic calibration performed in Section 4.1.2. Figure 5(a)–(c) shows the spatial distribution of grid cells with saturated soil states (as defined by $W > 0.95W_m$; refer to Section 2.1.2 and Table A2) after 72, 120 and 168 h of constant rainfall, respectively. At 72 h only a small number of grid cells (less than 1%) begin to become saturated in valleys. As rainfall proceeds, the number of grid cells being saturated increases at a linear rate up to 170 h (see Fig. 6). The saturation rate increases from 170 to 194 h; afterwards, all grid cells in the basin reach saturation. We also computed the spatial average of soil moisture values, plotted in a time series as a percentage of the maximum soil moisture storage (i.e. $(\bar{W}/\bar{W}_m) \cdot 100$; see Fig. 6). This curve shows a linear increase in the regional soil moisture contents until approximately 120 h. After this time, the regional soil moisture in the basin increases more gradually until all grid cells reach saturation at 194 h. After the rainfall is turned off at 200 h, we can see the number of saturated grid cells drops exponentially, and the regional soil moisture in the basin decreases linearly in response to the constant E_p of 5 mm/d.

In distributed hydrological models, soil moisture contents are typically determined by the spatial distribution and intensity of precipitation, infiltration characteristics and depth of the soil, land cover, and vegetation. The CREST model has demonstrated its ability to couple the rainfall–runoff generation to routing processes with the end result being a realistic pattern of grid cells becoming saturated in low-lying valleys first and then propagating upstream,

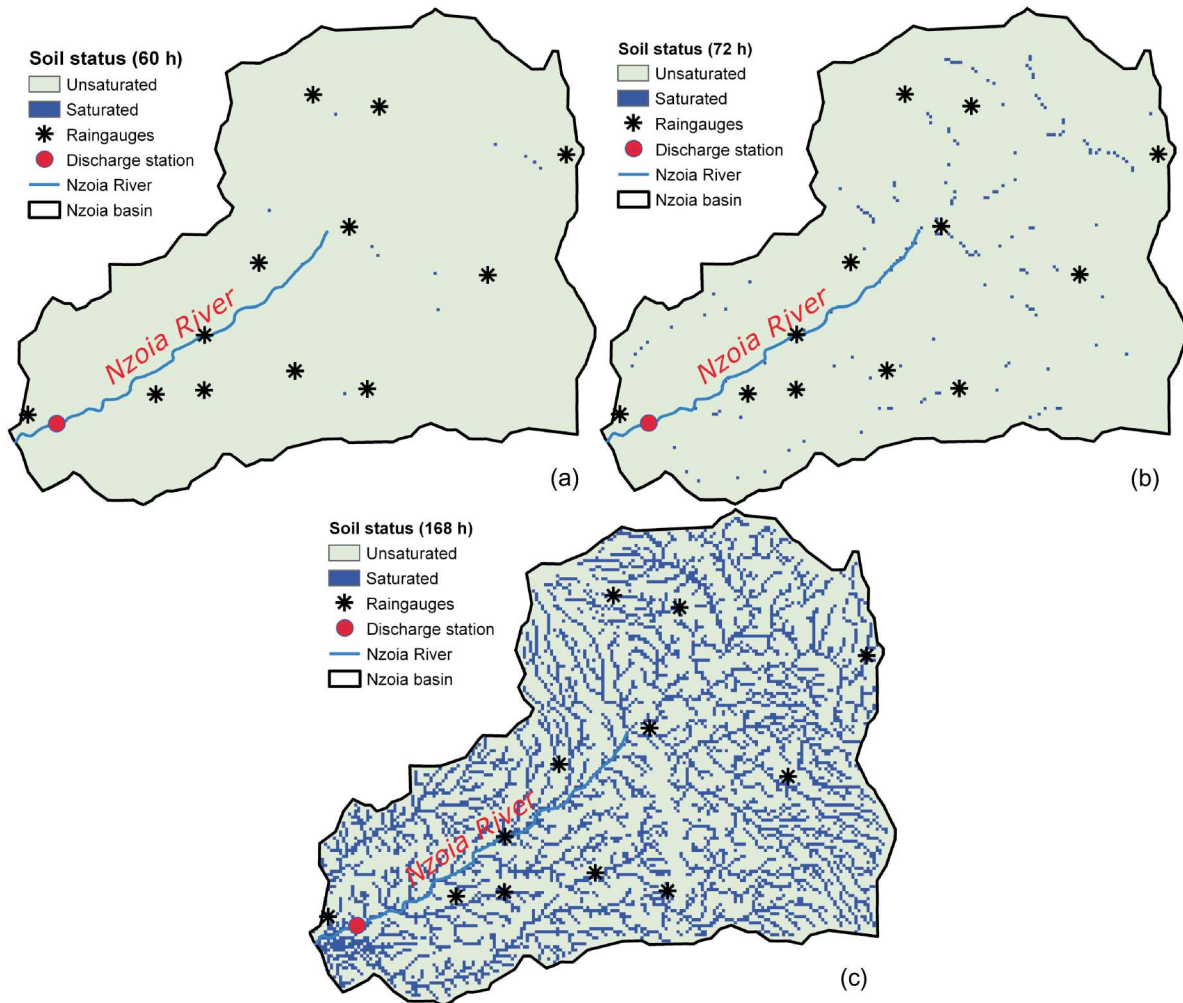


Fig. 5 Spatial distribution of grid cells with saturated soil states (as defined by $W > 0.95W_m$) after (a) 72, (b) 120 and (c) 168 h. This synthetic experiment assumed: (1) dry initial soil moisture conditions everywhere, (2) uniform precipitation at a rate of 10 mm/d in the first 200 h, (3) constant daily $E_p = 5$ mm/d, and (4) spatially uniform soil type and land cover.

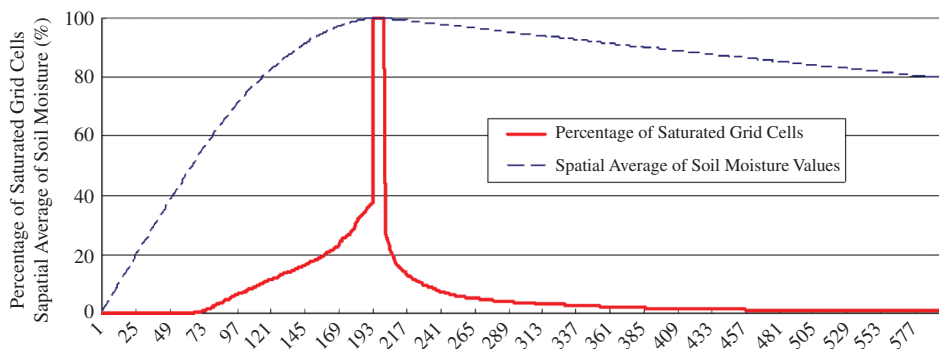


Fig. 6 Time series of percentage of saturated grid cells (as defined by $W > 0.95W_m$; solid line) and spatial average of soil moisture values (as defined by $\bar{W}/\bar{W}_m \cdot 100$; dashed line). Note that after uniform rainfall was input at a constant rate of 10 mm/d, it was suddenly stopped at the 200th hour. After this time, the percentage of saturated grid cells decreases exponentially due to runoff processes, while the spatial average of soil moisture values decreases more gradually in response to a 5 mm/d potential evapotranspiration rate.

patterns quite similar to the dynamic simulation study reported in Beven & Freer (2001). In essence, CREST accounts for the terrain dependence of soil moisture in addition to the other physical properties mentioned above. Future research will compare simulated soil moisture values with remotely-sensed or in situ values to determine whether the simulated soil moisture distribution is reasonably well represented by the CREST model and will guide further improvements if deemed necessary.

5 SUMMARY AND DISCUSSION

This paper describes the Coupled Routing and Excess Storage (CREST) model; a flexible spatially distributed hydrological model that is designed to simulate the spatiotemporal distribution of streamflow and soil moisture (and other hydrological variables) within a basin using data from remote sensing platforms (e.g. precipitation, land cover, elevation, etc.) and *in situ* instruments (e.g. rain gauges, soil moisture sensors, etc.). CREST was implemented in the Nzoia basin near Lake Victoria, Africa, and streamflow measurements were used to calibrate model parameters via an automatic calibration routine embedded in the CREST model code. The results during the validation period indicated very good performance with NSCE, Bias and correlation coefficient values of 0.71, -0.47% and 0.84, respectively. The display of spatially distributed flood information was demonstrated by showing the discharge at each grid cell in the basin. Future studies will examine the model performance in other basins where there are stream gauges at interior points. Another demonstration was provided to show the impact of coupling the rainfall-runoff generation and routing components on the spatiotemporal distribution of soil moisture values. The evolution of the soil moisture values appeared physically realistic with saturation occurring first in low-lying areas and propagating upstream. The validity of this behaviour will be further tested in a future study.

In summary, CREST has four desirable characteristics that contribute to its usefulness:

- (1) distributed rainfall-runoff generation and cell-to-cell routing;
- (2) coupling between the runoff generation and routing components via three feedback mechanisms; and
- (3) scalability through the representation of soil moisture variability (using a variable infiltration

curve) and routing processes (using linear reservoirs) at the sub-grid scale.

These characteristics make the CREST model suitable for multi-scale hydrological modelling applications ranging from global coverage (grid size of tens of kilometres) to regional coverage (grid size of 1 km to a few kilometres). The authors are currently implementing the CREST model for near-real time global streamflow simulations driven by remotely sensed precipitation estimates (<http://oas.gsfc.nasa.gov/CREST/global/>). More thorough validation of the model at multiple scales is required to assess its regional and global applicability.

As a newly developed model further research is required in many directions to enhance CREST, such as utilizing remote sensing data for developing distributed calibration strategies, detailed adjustment of the model parameters with the availability of field survey data, and further testing of the model performance in various hydro-climatic regions. Source code and a readme file for the Linux version of CREST are publicly accessible via email request or by visiting the NASA-SERVIR project website at www.servir.net or University of Oklahoma site at http://hydro.ou.edu/CREST_downloads.html.

Acknowledgements The financial support from NASA Applied Science Program SERVIR-Africa Project, from University of Oklahoma and NOAA/NSSL Director's Discretionary Research Fund is gratefully acknowledged. The authors also thank the RCMRD for providing gauged rainfall and streamflow observations over the Nzoia basin. The authors would like to extend their appreciation for support from grants no. 40801012, no. 40830639 of the NSFC (National Natural Science Foundation of China), and the Fundamental Research Funds for the Central Universities. Finally, we wish to thank the reviewers and editors for their encouraging and constructive comments.

REFERENCES

- Bates, G. T., F. Giorgi & S. W. Hostetler (1993) Toward the simulation of the effects of the Great Lakes on regional climate. *Mon. Weather Rev.* **121**, 1373–1387.
- Beck, M. B. (1987) Water quality modeling: a review of the analysis of uncertainty. *Water Resour. Res.* **23**, 1393–1442.
- Bergström, S. (1995) The HBV model. In: *Computer Models of Watershed Hydrology* (V. Singh, ed.), 443–476. Highlands Ranch, CO: Water Resources Publications.
- Beven, K. J. & Binley, A. M. (1992) The future of distributed models: model calibration and uncertainty prediction. *Hydrol. Processes* **6**, 279–298.

- Beven, K. & Freer, J. (2001) A dynamic TOPMODEL. *Hydrol. Processes* **15**(10), 1993–2011, doi:10.1002/hyp.252.
- Bonan, G. B. (1995) Sensitivity of a GCM simulation to inclusion of inland water surfaces. *J. Climate* **8**, 2691–2704.
- Branstetter, M. L. & Famiglietti, J. S. (1999) Testing the sensitivity of GCM-simulated runoff to climate model resolution using a parallel river transport algorithm. In: *Proc. 14th Conf. on Hydrology*, 391–392. Boston, MA: Am. Met. Soc.
- Brooks, S. H. (1958) A discussion of random methods for seeking maxima. *Operations Research* **6**, 244–254.
- Burnash, R. J. C. (1995) The NWS river forecast system—catchment modeling. In: *Computer Models of Watershed Hydrology* (V. Singh, ed.), 311–366. Highlands Ranch, CO: Water Resources Publications.
- Coe, M. T. (1997) Simulating continental surface waters: an application to Holocene Northern Africa. *J. Climate* **10**, 1680–1689.
- Dickinson, R. E. (1989) A regional climate model for the western united states. *Climate Change* **15**(1), 383–422.
- Friedl, M. A., McIver, D. K., Hodges, J. C. F., Zhang, X. Y., Muchoney, D., Strahler, A. H., Woodcock, C. E., Gopal, S., Schneider, A. & Cooper, A. (2002) Global land cover mapping from MODIS: algorithms and early results. *J. Remote Sens. Environ.* **83**(1–2), 287–302.
- Gupta, J. V., Sorooshian, S. & Yapo, P. O. (1998) Toward improved calibration of hydrologic models: multiple and noncommensurable measures of information. *Water Resour. Res.* **34**, 751–763.
- Hagemann, S. & Dümenil, L. (1998) A parameterization of the lateral waterflow for the global scale. *Climate Dynamics* **14**, 17–31.
- Hargreaves, G. H. & Samani, Z. A. (1982) Estimating potential evaporation. *J. Irrig. Drain. Engng ASCE* **108**(IR3), 223–230.
- Hostetler, S. W., Bates, G. T. & Giorgi, F. (1993) Interactive coupling of a lake thermal model with a regional climate model. *J. Geophys. Res.* **98**, 5045–5057.
- Kundzewicz, Z. W. & Stakhiv, E. Z. (2010) Are climate models “ready for prime time” in water resources management applications, or is more research needed? Editorial. *Hydrol. Sci. J.* **55**(7), 1085–1089.
- Lehner, B., Verdin, K. & Jarvis, A. (2008) New global hydrography derived from spaceborne elevation data. *Eos, Trans. Am. Geophys. Un.* **89**(10), 93–94.
- Li, L., Hong, Y., Wang, J., Adler, R., Policelli, F., Habib, S., Irwin, D., Korme, T. & Okello, L. (2009) Evaluation of the real-time TRMM-based multi-satellite precipitation analysis for an operational flood prediction system in Nzoia basin, Lake Victoria, Africa. *J. Natural Hazards* **50**(1), 2009, 109–123.
- Liang, X., Lettenmaier, D. P. & Wood, E. F. (1996) One-dimensional statistical dynamic representation of subgrid spatial variability of precipitation in the two-layer variable infiltration capacity model. *J. Geophys. Res.* **101**(D16), 21,403–21,422.
- Linsley, R. K., Kohler, M. A. & Paulhus, J. L. H. (1986) *Hydrology for Engineers*, 339–356. New York: McGraw-Hill.
- Liston, G. E., Sud, Y. C. & Wood, E. F. (1994) Evaluating GCM land surface hydrology parameterizations by computing river discharges using a runoff routing model. *J. Appl. Met.* **33**, 394–405.
- Miller, J., Russell, G. & Caliri, G. (1994) Continental scale river flow in climate models. *J. Climate* **7**, 914–928.
- Naden, P. S. (1993) A routing model for continental-scale hydrology. In: *Macroscale Modeling of the Hydrosphere* (W. B. Wilkinson, ed.) (Proc. Yokohama Symp., July 1993), 67–79. Wallingford: IAHS Press, IAHS Publ. 214.
- Nash, J. & Sutcliffe, J. (1970) River flow forecasting through conceptual models. Part I: A discussion of principles. *J. Hydrol.* **10**, 282–290.
- Osano, O., Nzyuko, D., Tole, M. & Admiraal, W. (2003) The fate of chloroacetanilide herbicides and their degradation products in the Nzoia Basin, Kenya. *Ambio: J. Hum. Environ.* **32**(6), 424–427.
- Priestley, C. H. B. & Taylor, R. J. (1972) On the assessment of surface heat flux and evaporation using large-scale parameters. *Mon. Weather Rev.* **100**, 81–92.
- Rabus, B., Eineder, M., Roth, A. & Bamler, R. (2003) The shuttle radar topography mission—a new class of digital elevation models acquired by spaceborne radar. *Photogramm. Remote Sens.* **57**, 241–262.
- Refsgaard, J. C. (1996) Terminology, modelling, protocol and classification of hydrological model codes. In: *Distributed Hydrological Modelling* (M. B. Abbott & J. C. Refsgaard, eds), 17–39. Amsterdam: Kluwer Academic Publishers, Water Science and Technology Library.
- Refsgaard, J. C. & Storm, B. (1995) MIKE SHE. In: *Computer Models of Watershed Hydrology* (V. Singh, ed.), 809–846. Highlands Ranch, CO: Water Resources Publications.
- Reichold, L., Zechman, E., Brill, E. & Holmes, H. (2010) Simulation–optimization framework to support sustainable watershed development by mimicking the predevelopment flow regime. *J. Water Resour. Plan. Manage.* **136**, 366.
- Singh, V. P. (ed.) (1995) *Computer Models of Watershed Hydrology*. Highlands Ranch, CO: Water Resources Publications.
- Sausen, R., Schubert, S. & Dümenil, L. (1994) A model of river runoff for use in coupled atmosphere–ocean models. *J. Hydrol.* **155**, 337–352.
- Vörösmarty, C. J., Moore, B., Grace, A., Gildea, M., Melillo, J., Peterson, B., Rastetter, E. & Steudler, P. (1989) Continental-scale model of water balance and fluvial transport: an application to South America. *Global Biogeochem. Cycles* **3**, 241–265.
- Vrugt, J. A., Diks, C. G. H., Gupta, H. V., Bouten, W. & Verstraten, J. M. (2005) Improved treatment of uncertainty in hydrologic modeling: combining strengths of global optimization and data assimilation. *Water Resour. Res.* **41**, W01017, doi:10.1029/2004WR003059.
- Woolhiser, D. A., Smith, R. E. & Goodrich, D. C. (1990) *KINEROS, Kinematic Runoff and Erosion Model: Documentation and User Manual*. US Dept of Agriculture – Agric. Research Service, USDA-ARS no. 77.
- Yilmaz, K. K., Vrugt, J. A., Gupta, H. V. & Sorooshian, S. (2010) Model calibration in watershed hydrology. Chapter 4 in: *Advances in Data-based Approaches for Hydrologic Modeling and Forecasting* (B. Sivakumar & R. Berndtsson, eds), 137–182. World Scientific Publishing.
- Zhao, R. J. (1992) The Xianjiang model applied in China. *J. Hydrol.* **135**(3), 371–381.
- Zhao Renjun, Zhang Yilin, Fang Leren, Liu Xinren & Zhang Quansheng (1980) The Xianjiang Model. In: *Hydrological Forecasting* (Proc. Oxford Symp., April 1980), 351–356. Wallingford: IAHS Press, IAHS Publ. 129.

APPENDIX

Table A1 Physically-based parameters.

Symbol	Unit	Brief description	Source for estimation
ACC	-	Accumulation grids	Derived from DEM
d	-	Vegetation coverage	Remote sensing
DEM	m	Digital elevation model	Remote sensing
Dire	-	Flow direction	Derived from DEM
K	mm h ⁻¹	Cell mean infiltration rate	Soil survey
l	m	Distance between cells	Derived from DEM
LAI	m ² m ²	Leaf area index	Remote sensing
S	degree	Slope between cells	Derived from DEM

Table A2 Parameters requiring optimization.

Symbol	Unit	Brief description	Default value
B	-	Exponent of variable infiltration curve	0.2
K_c	-	Coefficient of land cover's CIC	0.5
k_I	-	Interflow reservoir discharge parameter	0.1
k_O	-	Overland reservoir discharge parameter	0.5
k_X	-	Runoff velocity coefficient varying in overland, channel and interflow	50/100/15
Th	km ²	Threshold between overland and channel	30
W_{m1}	mm	Maximum cell mean water capacity of soil layer 1	20
W_{m2}	mm	Maximum cell mean water capacity of soil layer 2	50
W_{m3}	mm	Maximum cell mean water capacity of soil layer 3	80

Table A3 Inputs and outputs of the CREST model.

Symbol	Unit	Description
A	-	Upstream point of profile along several cells
CI	mm	Intercepted water in canopy layer
CIC	mm	Canopy interception capacity
E_a	mm h ⁻¹	Actual evaporation of bare soil
E_c	mm h ⁻¹	Actual evaporation from intercepted water in canopy layer
E_p	mm h ⁻¹	Potential evapotranspiration
E_{p1}	mm h ⁻¹	Potential evaporation from soil layer 1
E_{p2}	mm h ⁻¹	Potential evaporation from soil layer 2
E_{p3}	mm h ⁻¹	Potential evaporation from soil layer 3
E_{s1}	mm h ⁻¹	Actual evaporation from soil layer 1
E_{s2}	mm h ⁻¹	Actual evaporation from soil layer 2
E_{s3}	mm h ⁻¹	Actual evaporation from soil layer 3
i_m	mm	Maximum i of a cell
I	mm h ⁻¹	Infiltration water simulated from variable infiltration curve
\hat{I}	mm h ⁻¹	Adjusted I considering horizontal input water from routing
P	mm h ⁻¹	Precipitation
P_{soil}	mm h ⁻¹	Precipitation input to soil surface
\hat{P}_{soil}	mm h ⁻¹	Adjusted P_{soil} considering horizontal input water from routing
R	mm h ⁻¹	Excess rain generated by variable infiltration curve
R_O	mm h ⁻¹	Overland excess rain
R_I	mm h ⁻¹	Interflow excess rain
$R_{I,in}$	mm h ⁻¹	Interflow runoff entering a cell from routing
$R_{I,out}$	mm h ⁻¹	Interflow runoff leaving a cell
$R_{O,in}$	mm h ⁻¹	Overland runoff entering a cell from routing
$R_{O,out}$	mm h ⁻¹	Overland runoff leaving a cell
S_I	mm	Interflow reservoir storage
S_O	mm	Overland/channel reservoir storage
\hat{S}_O	mm	Adjusted S_O considering horizontal input water from routing
Sto	mm	Total cell water storage, including soil water and free water
T	h	Concentration time from cell to its downstream adjoining cell
W	mm	Total cell mean water of three soil layers
W_1	mm	Cell mean water in soil layer 1
W_2	mm	Cell mean water in soil layer 2
W_3	mm	Cell mean water in soil layer 3
W_m	mm	Maximum cell mean water capacity